Time-Frequency Analysis of Multiple Fringe and Nonsinusoidal Signals Obtained From a Fiber-Optic Vibration Sensor Using an Extrinsic Fabry–Pérot Interferometer

Tarun Kumar Gangopadhyay, *Student Member, IEEE*, Sivaji Chakravorti, *Senior Member, IEEE*, Saibal Chatterjee, and Kesab Bhattacharya, *Senior Member, IEEE*

***Abstract*—In the case of multiple fringes and complex frequency measurements, the frequency of the output signal changes rapidly when the vibration changes and frequency breakdown takes place at the turning point. For a particular vibration signature containing many frequency components at different time intervals, it is often difficult to trace the direction of the vibration as well as individual frequency peaks. In such cases, advanced signal-processing scheme is necessary to decode the vibration signature. This paper investigates the data interrogation technique for multifrequency and complex signals of surface vibration obtained from an extrinsic Fabry–Pérot interferometric sensor.**

In this paper, wavelet transform (WT)-based signal processing methodology has been employed to count of optical fringes with special reference to signals having subfringes. A WT-based tool has also been developed for unambiguous identification of frequency components from a nonsinusoidal vibration. The results of such WT-based analyses are presented, and merits as well as demerits of the proposed methods are discussed.

***Index Terms*—Extrinsic Fabry–Pérot interferometer (EFPI), fiber-optic vibration sensor, multifrequency vibration analysis, wavelet transform (WT).**

I. Introduction

A NOTABLE branch of rapidly developing photonics technology is the application of the Interferometric sensor using an optical fiber. These sensors have proved to be more sensitive than their electrical counterparts by several orders of magnitude [1]. For automatic monitoring of extended surfaces in real time without contact or perturbation, Fabry–Pérot interferometric (FPI) schemes in fiber optics are being established as versatile tools for fast and sensitive vibration analysis, which can also be combined with fiber-optic signal transmission for rugged performance in harsh engineering environments [2]–[13]. However, these sensors suffer from limitations in signal demodulation caused by phase ambiguity when the output phase difference exceeds one fringe period and in complex fringe counting in the case of multiple fringes.

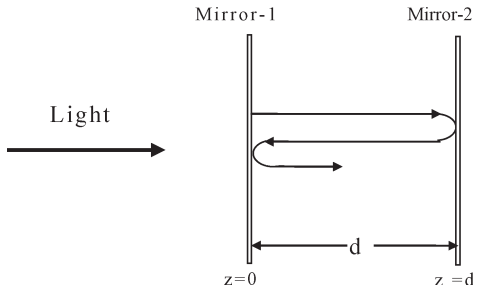

Fig. 1. Light rays perpendicular to the mirrors in an FP cavity.

It is well known that the difficulty of extracting the original displacement-versus-time characteristic from an interferometric sensor signal spanning multiple fringes is considerably higher when more than one frequency are present simultaneously. The measurement data reported in earlier papers [10]–[12] clearly show how difficult it would be to distinguish fringes on the basis of their amplitudes only. These reported traces are relatively simple and repetitive because of the presence of only one frequency in the displacement signal, which makes it easy to determine the turning points, at least, by visual examination. A real-world signal containing many frequency components would be much more difficult to interpret. Such multiple frequency signals have been analyzed in this paper, as it is thought to be necessary to make the sensor work satisfactorily in the real world. In such situations, multiresolution analysis using the continuous wavelet transform (CWT) has been carried out for complex and multiple fringe sensor signals by which the specific frequency components can be traced out. The CWT is a method of analysis that produces an output function of two variables, i.e., 1) time and 2) scale. Thus, CWT presents an image of the frequency-versus-time characteristics of signals. It is a qualitative tool for investigating nonstationary and time-dependent signal analysis [14].

The extrinsic FPI (EFPI), which is an extension of the classical technique, is attracting a great deal of interest in recent years. In the monitoring of extended surfaces, the EFPI cavity has been used to generate an optical interference signal between

Manuscript received September 15, 2004; revised February 11, 2006.

T. K. Gangopadhyay is with the Central Glass and Ceramic Research Institute, Council of Scientific and Industrial Research, Calcutta 700 032, India (e-mail: tkg@cgcri.res.in).

S. Chakravorti and K. Bhattacharya are with the Department of Electrical Engineering, Jadavpur University, Calcutta 700 032, India.

S. Chatterjee is with the Department of Electrical Engineering, North Eastern Regional Institute of Science and Technology (NERIST), Itanagar 791 109, India. He is also with the Department of Electrical Engineering, Jadavpur University, Calcutta 700 032, India.

Digital Object Identifier 10.1109/JLT.2006.872280

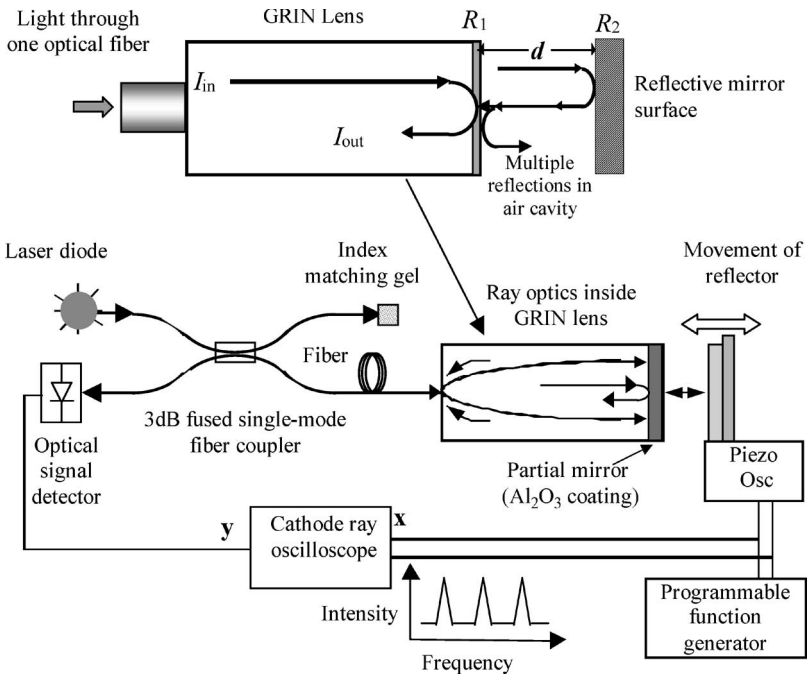

Fig. 2. Schematic of a reflective EFPI sensor connected with one fiber and measurement system [12].

two parallel highly reflective surfaces separated by a variable distance. The design and fabrication of an EFPI sensor, as well as the surface vibration captured from those fiber-optic sensors, have been reported by one of the authors in earlier communications [9]–[13], giving a working range of vibration up to 13.26 μm. In a recent communication [15], analysis of the sensor performance has been studied with the help of WT-based signal processing for the reduction of noise, identification of the frequency breakdown points of the signals, and by counting of the number of optical fringes after identification of the frequency breakdown points. It is a novel signal-decoding technique based on WT of optical data extracted from a noncontact vibration sensor using EFPI implemented using a single-mode fiber.

This paper, at first, presents new results for the reduction of noise from optical signals, identification of the frequency breakdown points, and counting of the number of optical fringes of signals that contain subfringes. It is followed by an investigation of the data interrogation technique for complex signals of surface vibration containing more than one sinusoidal component having different frequencies, as obtained from the FPI sensor designed and presented by one of the authors in an earlier work. Such signals having superimposed multiple frequency components are equivalent to nonsinusoidal vibrations. Thus, this paper demonstrates the method of analysis of EFPI output for nonsinusoidal vibration.

II. Principle of Operation of EFPI Vibration Sensor

The principle and design of a few configurations of FPI sensors using single-mode fiber have been reviewed in a reported paper [13]. The FP cavity is also the most convenient interferometric configuration as it is simply formed by the space between two typically parallel mirror surfaces (Fig. 1).

A monochromatic wave of free-space wavelength λ_0 is reflected within an FPI defined by two parallel mirror surfaces forming the FP cavity. The round-trip phase lag ϕ within such a cavity is given by [16], [17]

$$\varphi = \frac{2\pi(2nd\cos\,\theta)}{\lambda_0} = \frac{4\pi nd}{\lambda_0} \tag{1}$$

where n is the refractive index of the medium between the mirrors, d is the mirror separation, θ is the angle of incidence, and λ_0 is the propagating wavelength. If the cavity is air-filled $(n = 1)$ and the incident illumination is normal, then $\theta = 0$. With the help of the plane-wave approximation to the interference of superimposed signals from a two-wave interferometer [2], [7], the reflected intensity I_R from the FPI can be written as

$$I_R = |U_1 + U_2|^2 = A_1^2 + A_2^2 + 2A_1A_2\cos(\phi_1 - \phi_2) \tag{2}$$

where U_1 and U_2 are, respectively, the complex amplitudes for the reflected reference, A_1 and A_2 are the amplitudes of the reflected signals from two mirrors R_1 and R_2, and ϕ_1 and ϕ_2 are their corresponding phase lags. The subscripts 1 and 2 refer to the reference and sensing signals of the FPI, respectively. The static input mirror of the cavity provides the reference signal, whereas the second mirror, which is attached to the vibrating surface under test, provides the phase-modulated sensing signal.

The sensor system, as shown in Fig. 2 [12], incorporates illumination from a laser diode, gradient-index rod (GRIN) lens-based launch optics, and a 3-dB directional coupler. The focusing characteristics of the GRIN lens and recollection by

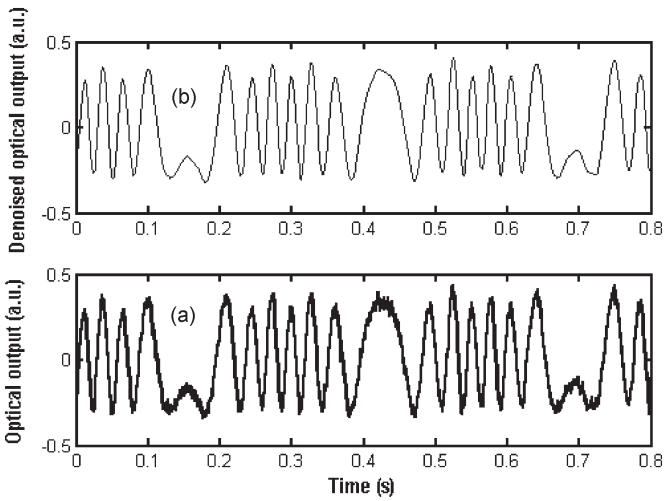

Fig. 3. (a) Real-time signal of the sensor to 1.86-kHz excitation that has multiple fringes along with subfringes (6.52 fringes), resulting in a vibration amplitude of 2.54 μm. (b) Denoised signal [15].

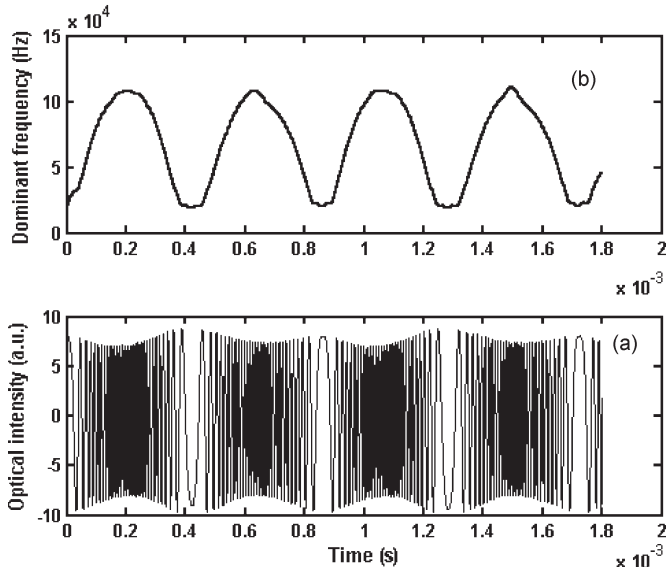

Fig. 4. (a) Real-time signal of the sensor to 1.18-kHz excitation that has integer-multiple fringes (30 fringes) resulting a vibration amplitude of 11.7 μm. (b) Determination of point of reflection.

the single-mode coupler fiber influence detection of interfering light from the FP cavity. Due to the vibration of mirror 2, the optical path difference (OPD) changes in the parallel direction and the intensity of the light cycles at wavelength λ_0, which produces a sine wave oscillation.

The propagating path length of optical signals l between two reflectors is equal to $2d$ (Fig. 2). For a two-wave interferometer, its output intensity I can be expressed as [1], [7]

$$I = I_0(1 + V\cos\,\varphi) \tag{3}$$

where I_0 is the average fringe intensity, and V is the fringe visibility. For a path length l, φ can be expressed as

$$\varphi = \frac{2\pi n l}{\lambda_0} \tag{4}$$

where n is the refractive index within the cavity of the EFPI.

The fringe visibility due to optical interference is the difference in intensities of the wave crests and troughs. In a perfectly coherent light beam, the fringe visibility is unity even if the OPD is long. At the output signal, one optical fringe is equivalent to a change in OPD of one wavelength, and the equivalent displacement recorded by a reflective FPI sensor in air $(n = 1)$ is one-half wavelength. The movement D of the test surface is therefore given by [7]

$$D = \frac{N\lambda_0}{2} \tag{5}$$

where N is the number of optical fringes, and λ_0 is the wavelength of laser light.

III. CWT

The work on signal demodulation technique using various algorithms in EFPI system for interferometric response is important nowadays. Several demodulation techniques have been reported to retrieve the cavity length, such as the peak-to-peak method in the wavelength domain, the discrete gap transform method in the spatial frequency domain, as well as the fast Fourier transform (FFT) method. FFT can make out whether a particular frequency component exists in a signal, but it is unable to provide information on time and frequency simultaneously, and thus, it is not suitable for the signals having time-varying frequency, i.e., nonstationary signals. CWT is a suitable method of analysis for nonstationary EFPI sensor signal and has been recently explored to retrieve the cavity length [15]. It is particularly useful for the signals for which one needs the information on identification of the breakdown points, trends, transient features, and discontinuities in higher derivatives [18].

WT is a useful tool for analysis of transients and nonstationary signals. It resolves the original wave into shifted and scaled version of the mother wavelet, which is a small wave having its energy concentrated in time. The CWT of a signal may be represented as [19]

$$\mathrm{CWT}_x^{\psi}(\tau, s) = \frac{1}{\sqrt{|s|}} \int x(t)\psi^* \frac{(t-\tau)}{s} dt \tag{6}$$

where τ and s are translation and scale, respectively, $\psi(t)$ is the mother wavelet function, and $*$ indicates complex conjugation. Variation of scale parameters produces dilated or compressed versions, whereas variation in translation parameters produces shifted versions of mother wavelet. Several mother wavelets are being used for CWT analysis, viz., Daubechies, Haar, Morlet, Symlet, etc., which are again divided into subtypes. However, the proposed scheme here is general in nature and is not limited to any particular mother wavelet.

In earlier work [20]–[22], the advantages of WT over FT, WT-based denoising, as well as different approaches to thresholding have been discussed. In the present denoising work, the WT parameters that have been varied to get best results are the following: 1) threshold type, which can be soft or hard; and 2) threshold selection rules, such as the one using the principle

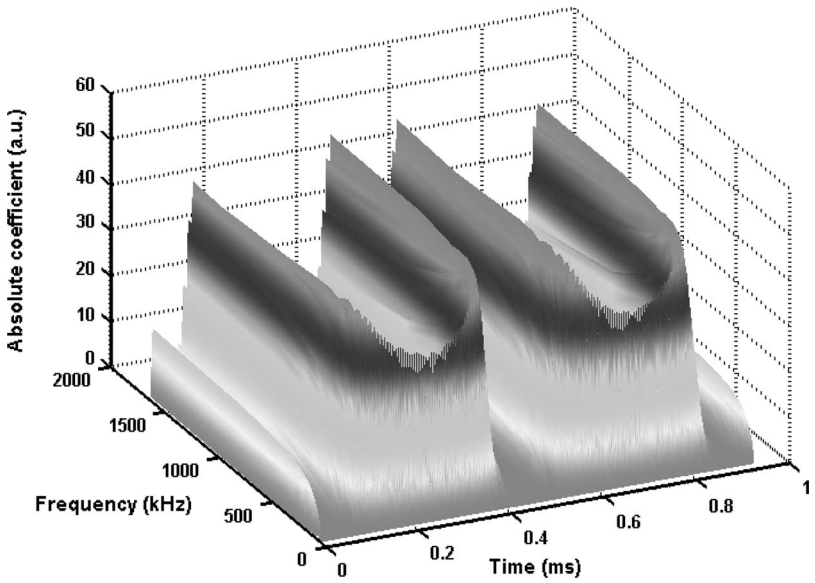

Fig. 5. Time-frequency representation (CWT coefficients using Morlet) of the sensor response to 1.27-kHz excitation resulting a vibration amplitude of 11.7 μm $\equiv$ 30 fringes.

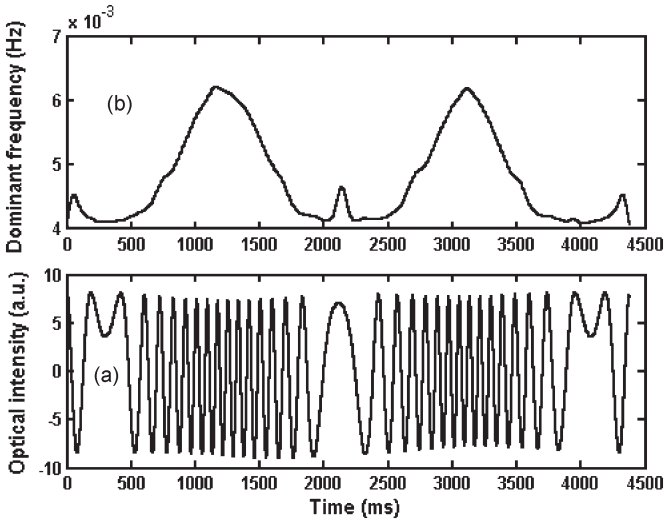

Fig. 6. (a) Real-time signal of the sensor to 1.32-kHz excitation that has multiple fringes along with subfringes (15.10 fringes), resulting in a vibration amplitude of 5.89 μm. (b) Determination of point of reflection.

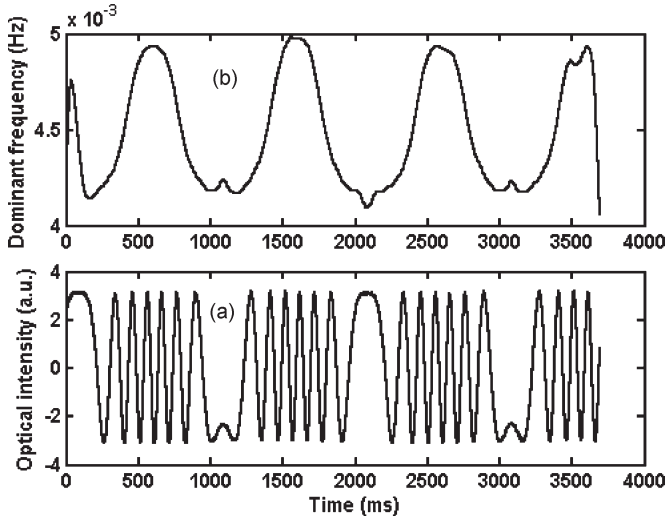

Fig. 7. (a) Real-time signal of the sensor to 1-kHz excitation that has multiple fringes along with subfringes (6.57 fringes), resulting in a vibration amplitude of 2.56 μm. (b) Determination of point of reflection.

of Stein's unbiased risk [23] (rigrsure), the heuristic version of the first option (heursure), the universal threshold sqrt$(2 * \log(\cdot))$ (sqtwolog), and the minimax thresholding (minimaxi). Multiplicative threshold rescaling has also been employed with the following option: 1) no scaling (one); 2) rescaling using a single estimation of level noise based on first-level coefficients (sln); and 3) rescaling using level-dependent estimation of level noise (mln).

Among the aforementioned parameters, selection of the mother wavelet and the selection of the number of levels are found to have the most significant effect on the WT-based denoising scheme. However, it may be stated here that an unambiguous method for the selection of the best suited mother wavelet has yet to be developed. Consequently, the selection of CWT parameters in this paper is based on the guidelines available from published literature.

IV. Methodology and Results

The experimental data have been obtained from the optical fiber sensor reported earlier [11], [12]. A piezoelectrical ceramic transducer (PZT) and a programmable function generator have been used to make the vibration of the reflective surface at a constant excitation during the experiment. A laser source of wavelength 780 nm has been used in the system. Sensor responses (real-time signal of the sensor) are captured for different excitations and are analyzed in this paper.

A. WT-Based Analysis of Optical Signal for Single Frequency Sinusoidal Exciting Vibration

A noisy optical signal with multiple fringes along with subfringes has been shown in Fig. 3(a). The presence of

significant amount of noise is clearly shown in Fig. 3(a), and it is thus denoised through the wavelet-based denoising tool. The denoised responses are shown in Fig. 3(b). In the denoising scheme of the Matlab wavelet toolbox, open- and closed-loop approaches [15] are applied. Selection of the threshold rule utilized for denoising is "rigrsure," the threshold type is "soft," the name of the wavelet is "Bior6.8," the level is "five," and multiplicative threshold rescaling is "one."

For signals having multiple fringes with different frequency components at different time intervals, it is often difficult to trace the direction of the vibration. In such cases, multiresolution analysis using WT can be employed by which the frequency components may be traced out. One such measured data that has integer-multiple fringes (30 fringes) is presented in Fig. 4(a). The trace shown in Fig. 4(a) is relatively simple and repetitive because of the single frequency (1.18 kHz) displacement signal, making it easy to determine the turning points by visual examination. Real-time signals containing many frequency components would be much more difficult to interpret. Hence, the CWT of the signal is taken using an appropriate mother wavelet, e.g., Morlet wavelet. Time-frequency representation of the signal of Fig. 4(a) by determination of point of reflection is shown in Fig. 5. The scale of maximum WT coefficient is determined at each time instant and the inverse of this scale in the dominant frequency at each time instant. The plot of dominant frequency versus time is shown in Fig. 4(b). From the plot of dominant frequency versus time, it may be seen that it is repetitive in nature with consecutive maximum and minimum. The point of lowest dominant frequency corresponds to the point of reflection of optical signal, which is also corroborated from the plot of optical signal against time of Fig. 4. The values of lowest dominant frequency and the corresponding time of occurrences can be found from the plot.

Fig. 6(a) shows the EFPI response to 1.32-kHz excitation that has multiple fringes along with subfringes (15.10 fringes) corresponding to a 5.89-μm vibration amplitude, and the corresponding plot of dominant frequency versus time is shown in Fig. 6(b). Similarly, Fig. 7(a) shows the EFPI response to 1.3-kHz excitation that has multiple fringes along with subfringes (6.57 fringes) corresponding to a 2.56-μm vibration amplitude, and the corresponding plot of dominant frequency versus time is shown in Fig. 7(b). Both Figs. 6(b) and 7(b) show that subfringes result in a kink at the minima of the dominant frequency-versus-time plot. In other words, kinks at the minima of dominant frequency-versus-time plots are signatures of the subfringes of EFPI signals. It becomes eminently clear when Figs. 6(b) and 7(b) are compared with Fig. 4(b). For signals having subfringes, the average of the two minima on the two sides of the kink is taken as the point of reflection. In addition to the counting of the number of complete fringes (integer fringes) between two successive points of reflection, the peak-to-peak magnitude of the subfringe at the point of reflection is calculated, and its ratio with respect to the full peak-to-peak magnitudes of a complete fringe is determined, which gives excellent resolution in the identification of subfringes. The algorithm of such complete fringe counting along with subfringe counting is shown in Fig. 8, which is based on Matlab–Simulink coding [15]. The numbers of fringes as counted by the developed algorithm are 15.10 and 6.57 for the signals shown in Figs. 6(a) and 7(a), respectively.

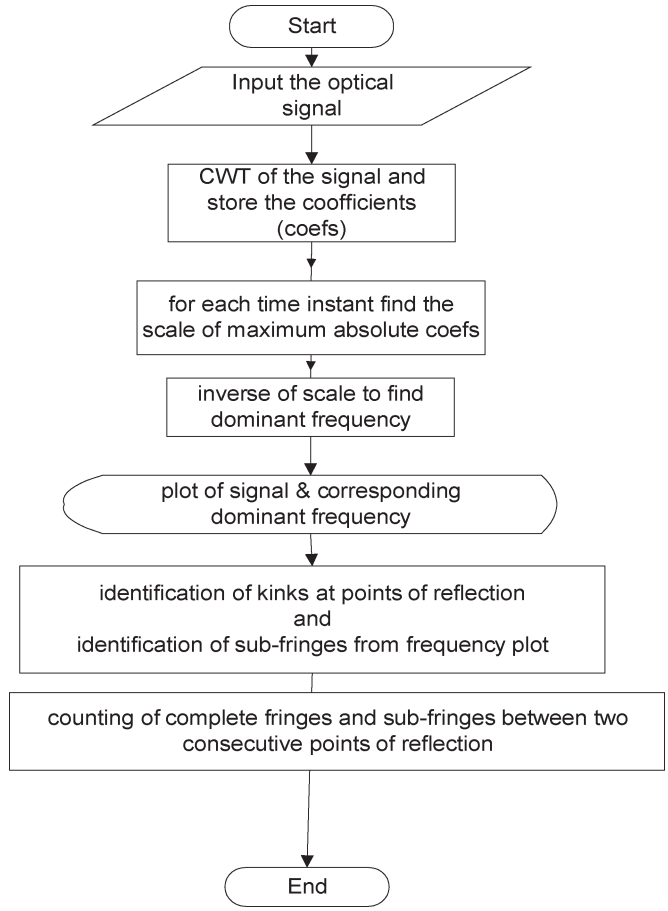

Fig. 8. Algorithm for counting of complete fringes and subfringes.

B. WT-Based Analysis of Optical Signal for Superimposed Multiple Frequency Sinusoidal Exciting Vibration

Three sensor's responses (real-time signal of the sensor) are illustrated in Fig. 9(a)–(c), respectively, for three different excitations [11], [12]. Fig. 9(a) shows an optical output with 34 fringes at 1.18-kHz excitation, which is equivalent to the vibration amplitude of 13.23 μm. Fig. 9(b) shows an output with 22 fringes at 1.275-kHz excitation corresponding to a vibration amplitude of 8.58 μm. Fig. 9(c) shows an output with nine fringes at 1.62-kHz excitation equivalent to the vibration amplitude of 3.51 μm. Fig. 9(d) shows the superimposed nonsinusoidal vibration due to the aforementioned three sinusoidal excitations. Generation of such nonsinusoidal vibration signal is quite realistic in nature, as any real-life continuous nonsinusoidal signal can be resolved into many sinusoidal components. In this paper, nonsinusoidal vibration signals are created using known sinusoidal vibration signals, such that the accuracy of the developed methodology can be ascertained.

Wavelet analysis of such a nonsinusoidal vibration signal has been carried out using the Matlab wavelet toolbox [19]–[24]. At the beginning of the analysis, the CWT of the nonsinusoidal signal is performed, and the coefficients and frequencies at

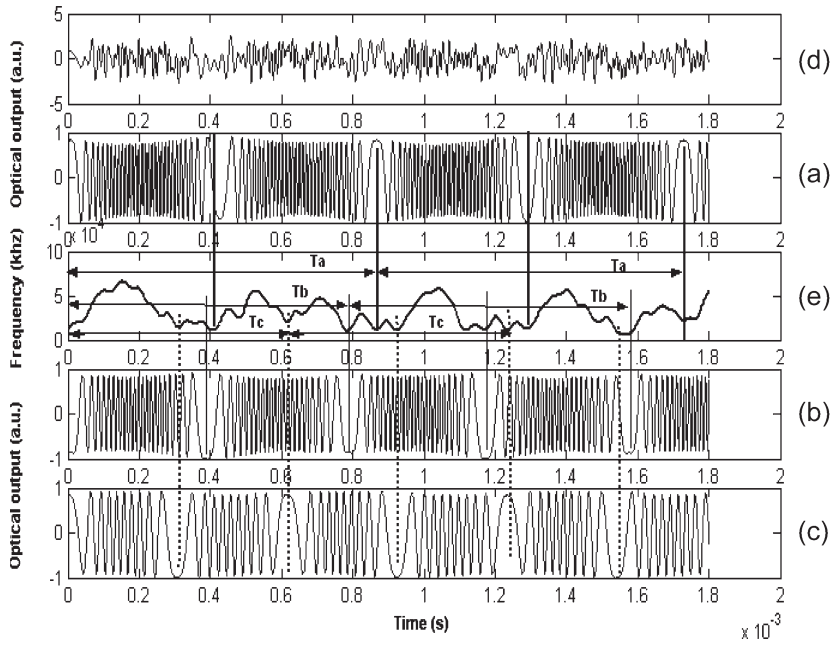

Fig. 9. Determination of the turning points from a nonsinusoidal signal having three superimposed frequencies and, thereby, identification of the number of constituent signals. (a) Real-time signal of the sensor at 1.18-kHz excitation with 34 fringes, (b) real-time signal of the sensor to 1.27-kHz excitation with 22 fringes, (c) real-time signal of the sensor to 1.62-kHz excitation with nine fringes, (d) nonsinusoidal signal due to superposition of three signals with three frequencies and amplitudes, and (e) minimum frequency curve obtained from CWT results from which the constituent signals could be traced out. T_a, T_b, and T_c are the time periods of signals (a), (b), and (c), respectively.

TABLE I
TIME OF OCCURRENCES OF TURNING POINTS AS OBTAINED FROM LOW-FREQUENCY PEAKS OF MINIMUM FREQUENCY CURVE FOR IDENTIFICATION OF CONSTITUENT SIGNALS HAVING 34, 22, AND NINE FRINGES

Signal Sl. No.	1st Turning point (in seconds)	2nd Turning point (in seconds)	3rd Turning point (in seconds)	4th Turning point (in seconds)	5th Turning point (in seconds)	Calculated frequency	Actual frequency
1.	0.00041	0.0008675	0.001293	0.001734		1.1527 kHz	1.18 kHz (34 fringes)
2.	0.00041	0.0007845	0.0011735	0.0015715		1.2747 kHz	1.275 kHz (22 fringes)
3.	0.0003085	0.0006155	0.0009255	0.001234	0.0015715	1.6247 kHz	1.62 kHz (9 fringes)

each time instant are stored. At each time instant, the lowest dominant frequency is identified, which is the minimum frequency for which there exists a positive peak coefficient. Such lowest dominant frequencies are plotted against time to give a curve named "minimum frequency curve." Fig. 9(e) shows the minimum frequency curve from which the turning points of the frequencies can be traced out. At the turning point of each constituent signal, the frequency is minimum. Hence, in the minimum frequency curve, a trough is expected at all the turning points of the constituent signals. The time instants of the troughs of the minimum frequency curve are noted and studied to check whether any repetitive series can be formed out of the noted time instants. As the nonsinusoidal signal comprises multiple sinusoidal signals of different frequencies, it is expected that the number of repetitive time series having distinctly different time periods would match with the number of constituent signals.

The aforementioned aspect can be better explained with the help of Table I. The values of significant low frequencies are identified from the troughs on the minimum frequency curve, and the corresponding times of occurrences are noted. The first row of Table I shows that four distinct time instants are present, which are nearly equidistant. The corresponding time period T_a is marked in Fig. 9. The frequency calculated from the average time period of this series closely matches with the actual frequency of one constituent signal, i.e., 1.18 kHz corresponding to 34 fringes. Similarly, the second and third rows also show that there are two other distinctly separate repetitive series of time instants having two nearly equal time periods. The frequency calculated from the average time period

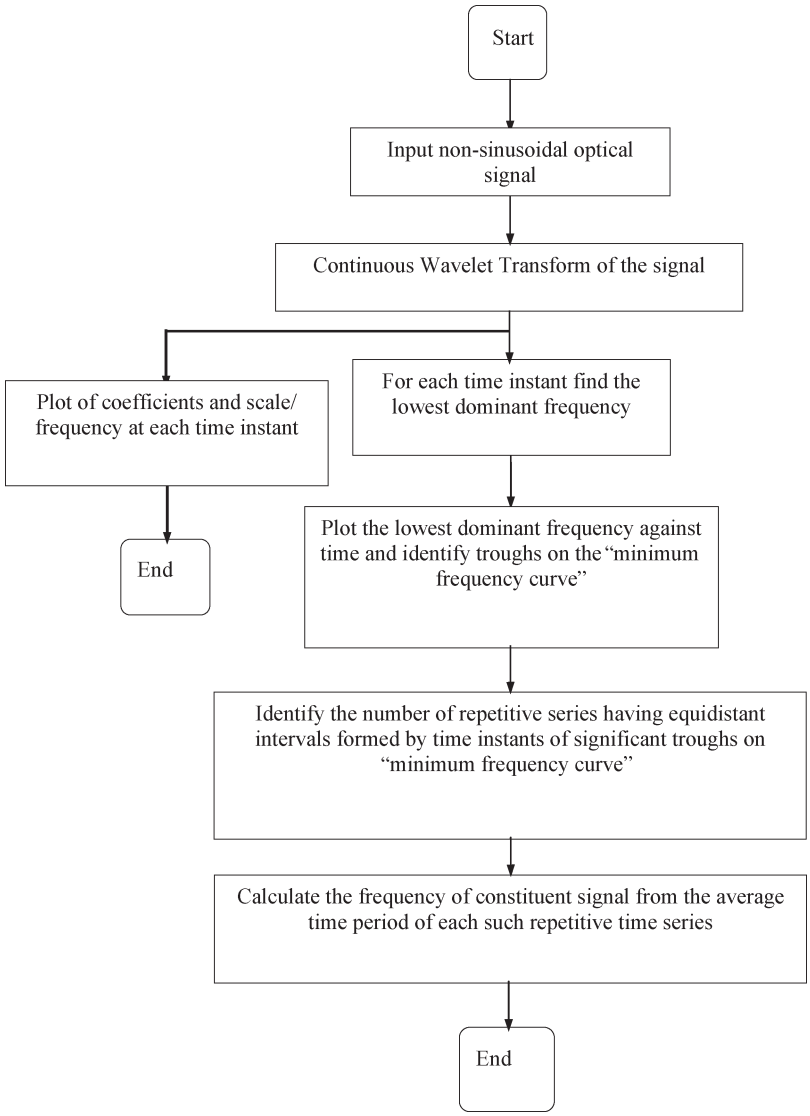

Fig. 10. Algorithm to identify constituent signals of different frequencies out of a nonsinusoidal signal of the sensor response based on WT analysis.

of row 2 matches the actual frequency of another constituent signal, i.e., 1.275 kHz corresponding to 22 fringes, and the frequency calculated from row 3 matches well with the actual frequency of the third constituent signal, i.e., 1.62 kHz that corresponds to nine fringes. The time periods of the second and third data rows T_b and T_c, respectively, are also marked in Fig. 9. In this way, it is seen that all the constituent signals having different frequencies can be clearly identified by the method proposed. Fig. 10 presents the algorithm based on the WT of the sensor response for identification of the constituent signals of different frequencies out of a nonsinusoidal sensor response.

Another result similar to the one presented in Fig. 9 is shown in Fig. 11. In this case, the nonsinusoidal multifrequency signal is obtained by the superposition of three signals that have 34, 22, and seven fringes, respectively. The minimum frequency curve shown in Fig. 11(e) is obtained following the same procedure described earlier for Fig. 9. It again clearly shows the turning points of the frequencies, as distinctly different repetitive time series are formed by equidistant significant troughs of the curve. Table II presents the time instants of the repetitive turning points of the constituent signals, as obtained from the significant troughs of the minimum frequency curve of Fig. 11(e). The number of such repetitive time series is found to be equal to the number of constituent signals having different frequencies, and the corresponding time periods are marked in Fig. 11(e). The calculated frequencies from the average time periods of each such time series match very well with the actual frequency of constituent signals, as mentioned in Table II.

V. Conclusion

The optical interference signals of an EFPI sensor have been analyzed to study vibration measurement performance. Elimination of noise from optical signals and counting of fringes, particularly for signals having subfringes, are well demonstrated using WT-based tool. A method based on WT is also processed for identification of constituent signals having different frequencies out of a nonsinusoidal optical sensor response.

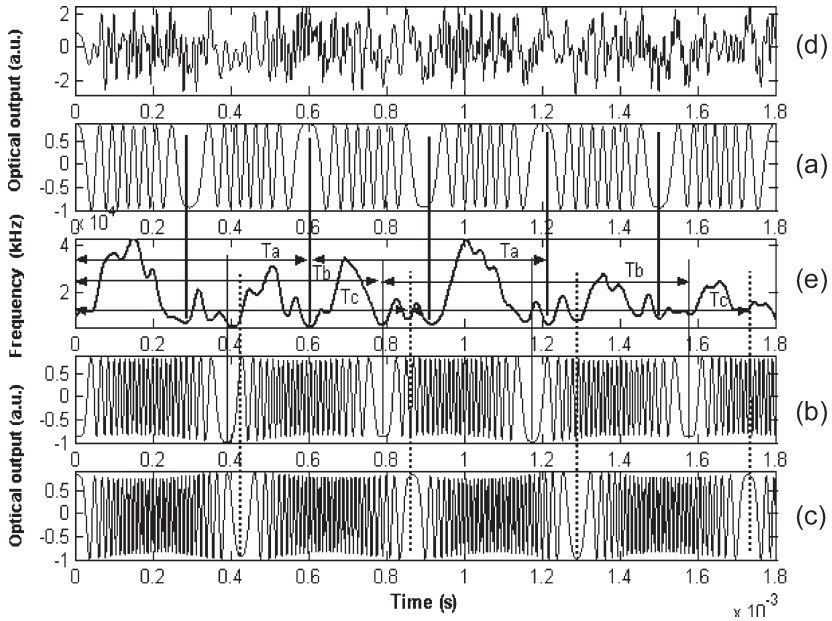

Fig. 11. (a) Real-time signal of the sensor to 1.62-kHz excitation indicating seven fringes, (b) 1.27-kHz excitation indicating 22 fringes, (c) 1.18-kHz excitation indicating 34 fringes, (d) nonsinusoidal signal due to superposition of three signals having three frequencies and amplitudes, and (e) minimum frequency curve obtained from CWT from which the constituent signals could be traced out. T_a, T_b, and T_c are the time periods of signals (a), (b), and (c), respectively.

TABLE II
TIME OF OCCURRENCES OF TURNING POINTS AS OBTAINED FROM LOW-FREQUENCY PEAKS OF MINIMUM FREQUENCY CURVE FOR IDENTIFICATION OF CONSTITUENT SIGNALS HAVING 34, 22, AND SEVEN FRINGES

Signal Sl. No.	1st Turning point (in seconds)	2nd Turning point (in seconds)	3rd Turning point (in seconds)	4th Turning point (in seconds)	5th Turning point (in seconds)	Calculated frequency	Actual frequency
1.	0.000411	0.000854				1.171 kHz	1.18 kHz (34 fringes)
2.	0.000411	0.0007915	0.001219	0.00158		1.2634 kHz	1.275 kHz (22 fringes)
3.	0.000294	0.000605	0.000854	0.001219	0.0015015	1.652 kHz	1.62 kHz (7 fringes)

The method has been tested successfully for nonsinusoidal sensor responses comprising three different frequency signals. Multiple frequency components have been separated by their repetitive time series having distinctly different time periods that match with the frequency of actual signals. Although the developed methodology has been tested using nonsinusoidal signals having three sinusoidal components, it is not limited in capacity but is general in nature and can also be used for a higher number of constituent signals.

However, it has been noted that the proposed method does not perform well in the following cases. First, it will be very difficult to separate the turning points of two different constituent signals if they are very close to each other. This is evident from the data of the first column of Tables I and II, where it may be seen that the first turning point of 34 and 22 fringe signals are identified at the same time instant. However, Figs. 9 and 11 show that these two turning points are not same but are very close to each other. Second, difficulty will also arise if the frequency of one constituent signal is an integer multiple or submultiple of another constituent signal. Further research is continuing to find solutions to these problems.

ACKNOWLEDGMENT

The authors would like to thank Dr. H. S. Maiti, Director, Central Glass and Ceramic Research Institute (CGCRI), Council of Scientific and Industrial Research, Calcutta, India, for his kind permission to communicate this paper for possible publication and Dr. S. Bandyopadhyay, K. Dasgupta, and Dr. S. K. Bhadra, CGCRI, for their help and suggestions during the analysis.

One of the authors (T. K. Gangopadhyay) would also like to thank the Australian Agency for International Development and the Australian GIRD project 16045 for the practical setup to

conduct experiments at the School of Electrical and Information Engineering, University of Sydney, Sydney, Australia, and Dr. P. J. Henderson, Prof. A. D. Stokes, and Dr. G. Town for their helpful assistance during the experiments.

REFERENCES

[1] K. T. V. Grattan and B. T. Meggitt, *Optical Fiber Sensor Technology*. London, U.K.: Chapman & Hall, 1995.
[2] T. Yoshino, K. Kurosawa, K. Itoh, and T. Ose, "Fiber-optic Fabry–Pérot interferometer and its sensors applications," *IEEE J. Quantum Electron.*, vol. QE-18, no. 10, pp. 626–665, Oct. 1982.
[3] R. Kist, S. Ramkrishanan, and H. Wölfelschneider, "The fiber Fabry–Pérot and its applications as a fiber-optic sensor element," in *Proc. SPIE*, 1985, vol. 586, pp. 126–133.
[4] D. A. Jackson and J. D. C. Jones, "Fibre optic sensors," *Opt. Acta*, vol. 33, no. 12, pp. 1469–1503, 1986.
[5] F. Farahi, T. P. Newson, J. D. C. Jones, and D. A. Jackson, "Coherence multiplexing of remote fibre optic Fabry–Pérot sensing system," *Opt. Commun.*, vol. 65, no. 5, pp. 319–321, Mar. 1988.
[6] G. L. Mitchell, "A review of Fabry–Pérot interferometric sensors," *Proc. 6th Int. Conf. OFS*, H. J. Arditty, J. P. Dakin, and R. Th. Kersten, Eds., 1989, pp. 450–457.
[7] K. A. Murphy, M. F. Gunther, A. M. Vengsarkar, and R. O. Claus, "Quadrature phase-shifted, extrinsic Fabry–Pérot optical fiber sensors," *Opt. Lett.*, vol. 16, no. 4, pp. 273–275, Feb. 1991.
[8] P. J. Henderson, Y. J. Rao, and D. A. Jackson, "Simultaneous dynamic-strain and temperature monitoring using a wavelength-multiplexed fibre-Fabry–Perôt array with low-coherence interrogation," in *Proc. 12th Int. Conf. Opt. Fibre Sens., OSA Tech. Dig. Ser*. Washington, DC: OSA, 1997, vol. 16, pp. 56–59.
[9] T. K. Gangopadhyay, P. J. Henderson, and A. D. Stokes, "Vibration monitoring using a dynamic proximity sensor with interferometric encoding," *Appl. Opt., Opt. Soc. Amer.*, vol. 36, no. 22, pp. 5557–5561, Aug. 1, 1997.
[10] T. K. Gangopadhyay and P. J. Henderson, "Vibration: History and measurement using an extrinsic Fabry–Pérot sensor with solid-state laser interferometry," *Appl. Opt.*, vol. 36, no. 12, pp. 2471–2477, 1999.
[11] T. K. Gangopadhyay, G. Town, and A. D. Stokes, "Noncontact vibration monitoring technique using a single-mode fibre sensor," in *Proc. ACOFT*, Sydney, Australia, Jul. 4–9, 1999.
[12] T. K. Gangopadhyay, "Non-contact vibration measurement based on extrinsic Fabry–Pérot interferometer implemented using arrays of single-mode fibres," *Meas. Sci. Technol.*, vol. 15, no. 5, pp. 911–917, May 2004.
[13] ——, "Prospects for fibre Bragg gratings and Fabry–Pérot interferometers in fibre-optic vibration sensing—A review," *Sens. Actuators A, Phys.*, vol. 113, no. 1, pp. 20–38, May 2004.
[14] J. Sadowsky, "Investigation of signal characteristics using the continuous wavelet transform," *Johns Hopkins APL Tech. Dig.*, vol. 17, no. 3, pp. 258–269, 1996.
[15] T. K. Gangopadhyay, S. Chakravorti, K. Bhattacharya, and S. Chatterjee, "Wavelet analysis of optical signal extracted from a non-contact fibre-optic vibration sensor using extrinsic Fabry–Pérot interferometer," *Meas. Sci. Technol.*, vol. 16, no. 5, pp. 1075–1082, May 2005.
[16] B. E. A. Saleh and M. C. Teich, *Fundamentals of Photonics*. New York: Wiley, 1991.
[17] J. M. Vaughan, *The Fabry–Pérot Interferometer*. Bristol, U.K.: Adam Hilger, 1989.
[18] L. Dokos, M. Mowlem, and A. Chambers, "Application of time-frequency analysis on obtained data from a low velocity impact using fibre optic sensors," in *Proc. PG Conf. Eng. Mater.*, 2001, pp. 27–28.
[19] R. K. Young, *Wavelet Theory and its Applications*. Norwell, MA: Kluwer, 1993.
[20] I. Shim, J. J. Shoragan, and W. H. Siew, "Detection of PD utilising digital signal processing methods, part 3: Open loop noise reduction," *IEEE Electr. Insul. Mag.*, vol. 17, no. 1, pp. 6–13, Jan./Feb. 2001.
[21] X. Ma, C. Zhao, and I. J. Kemp, "Investigation into the use of wavelet theory for partial discharge pulse extraction in electrically noisy environments," *IEEE Electr. Insul. Mag.*, vol. 18, no. 2, pp. 37–45, Mar./Apr. 2002.
[22] J. Ramirez-Nino, S. Rivera-Castaneda, V. R. Garcia-Colon, and V. M. Castano, "Analysis of partial discharges in insulating materials through the wavelet transform," *Comput. Mater. Sci.*, vol. 9, no. 3–4, pp. 379–388, 1998.
[23] M. Misti, Y. Misti, G. Oppenheim, and J. Poggi, *Wavelet Toolbox Manual—User's Guide*. Natick, MA: The Math Works Inc., 1996.
[24] I. Shim, J. J. Shoragan, and W. H. Siew, "Digital signal processing applied to the detection of partial discharge: An overview," *IEEE Electr. Insul. Mag.*, vol. 16, no. 3, pp. 6–12, May/Jun. 2000.

Tarun Kumar Gangopadhyay (S'03) was born in Gopalpur, India, on January 7, 1959. He received the Bachelor's degree in electrical engineering (first class honors) and the Master's degree in electrical engineering (first class honors) from Jadavpur University, Calcutta, India, in 1989 and 1991, respectively, and the Ph.D. degree in the field of fiber-optic sensor from the University of Sydney, Sydney, Australia, in December 2005. He carried out research in the area of fiber-optic transducers in his thesis submitted for the Master's degree. His Ph.D. dissertation was entitled "Measurement of vibration using optical fibre sensors."

He joined the Dishergarh Thermal Power Station, India, working in the area of power generation and transmission. Later, he was appointed as an Electrical Engineer in the Central Glass and Ceramic Research Institute (CGCRI), Council of Scientific and Industrial Research (CSIR), Calcutta, where he carried out research work in the development of varistor materials for high-voltage applications. From 1995 to 1999, he was in Australia under the Australian Agency for International Development scholarship for commonwealth countries, where he was involved in the research and development of optical fiber vibration sensors for electrical power industry with the High Power Testing and Optical Fibre Sensors Group, School of Electrical and Information Engineering, University of Sydney. He worked there in the field of intrinsic and extrinsic single-mode fiber-based sensors and fiber-optic interferometry. He has authored several journal papers and international conference proceedings. He has done some theoretical research work and has published jointly with the University of Kent, Canterbury, U.K. He is currently involved in the R&D work of optical fiber sensors, fiber Bragg grating (FBG) sensors for smart structures, FBG sensors for power line application, fiber fabrication and characterization, fiber-optic amplifiers, and fiber-optic components such as bidirectional couplers, wavelength division multiplexing couplers in CGCRI, and CSIR. His current research interests are the development of FBG sensors, biomedical sensors, and polarization-maintaining fiber couplers for gyro applications.

Dr. Gangopadhyay is a member of the Optical Society of America (OSA), and the Institution of Engineers, India. He was the recipient of various awards and prizes for his research work with the University of Sydney and the Australian Photonics Society.

Sivaji Chakravorti (M'89–SM'02) received the B.E.E., M.E.E., and Ph.D. degrees from Jadavpur University, Kolkata, India, in 1983, 1985, and 1993, respectively.

Since 1985, he has been a full-time Faculty Member of the Department of Electrical Engineering, Jadavpur University, where he is currently a Professor of electrical engineering. In 1984, he was with the Indian Institute of Science, Bangalore, India, as an Indian National Science Academy Visiting Fellow. He was a Humboldt Research Fellow at the Technical University Munich, Munich, Germany, in 1995–1996 and 1999. He served as a Development Engineer with Siemens AG, Berlin, Germany, in 1998. He was a Humboldt Research Fellow at ABB Corporate Research, Ladenburg, Germany, in 2002. In 2003, he was a U.S.-NSF Guest Scientist at the Virginia Polytechnic Institute and State University, Blacksburg. He has published about 60 research papers and has authored a book. His current fields of interest are numerical field computation, computer-aided design and optimization of insulation systems, application of artificial intelligence in high-voltage systems, condition monitoring of large electrical equipment, and electromagnetic compatibility.

Dr. Chakravorti received the Technology Day Award of the AICTE for best project work in 2003.

Saibal Chatterjee was born in Kolkata, India, in 1969. He received the B.E.E. degree from Burdwan University, Burdwan, India, in 1990 and the M.E.E. degree from Jadavpur University, Kolkata, in 1994.

Currently, he is a Lecturer with the Department of Electrical Engineering, North Eastern Regional Institute of Science and Technology (NERIST), Itanagar, India. He is presently involved in doctoral research at Jadavpur University. He has more than three years of industrial experience. His current research involves high-voltage switching transients and advanced signal processing techniques in high-voltage engineering.

Kesab Bhattacharya (M'95–SM'03), photograph and biography not available at the time of publication.